

Characterization and Formability of Titanium/Aluminum Laminate Composites Fabricated by Hot Pressing

Liang Qin, Hui Wang, Shengqiang Cui, Qian Wu, Minyu Fan, Zonghui Yang, and Jie Tao

(Submitted December 27, 2015; in revised form April 21, 2017; published online June 16, 2017)

The Ti/Al laminate composites were prepared by hot pressing to investigate the forming performance due to the corresponding potential applications in both the aerospace and auto industry. The bonding interface morphology and element distributions were characterized by SEM and EDS. The phase constituent was detected by XRD. It was observed that these composites presented good bonding interfaces between Ti and Al layers, and no low-sized voids and intermetallic compounds formed at the interface. In addition, the formability of these laminate composites was studied by the uniaxial tension tests, the limit drawing ratio (LDR) and the forming limit curve (FLC) experiments, respectively. The results indicated that the flow stress increased along with the strain rate increment. A constitutive equation was developed for deformation behavioral description of these laminate composites. The LDR value was 1.8, and the most susceptible region to present cracks was located at the punch profile radius. The forming limit curve of the laminate composites was located between the curves of titanium and aluminum and intersected with the major strain line at approximately 0.31. The macroscopic cracks of the FLC sample demonstrated a saw-toothed crack feature.

Keywords characterize, formability, forming limit curve (FLC), limit drawing ratio (LDR), Ti/Al laminate composites, uniaxial tension test

1. Introduction

During the recent decades, composites with a laminate (or multilayered) structure have gained popularity due to the corresponding superior physical properties, chemical advantages and impressive mechanical properties (Ref 1-3). Therefore, the studies in the field of composites are proven to be quite promising and attractive. Currently, many studies have been executed on the laminate composites preparation and properties (Ref 4-8). A high number of laminate composites have been widely studied, such as Ti/Al (Ref 9), Al/Fe (Ref 10), Al/Mg (Ref 11), Nb/Al (Ref 12), Cu/Al (Ref 13) and Cu/Ti (Ref 14). Among these laminate composites, the Ti/Al material binary system, prepared by pure Ti and Al, has received a high attention. Following all Al foils reaction

during heat treatment, the Ti/Al laminate composites can be transformed into the Ti/Al_xTi_y laminate composites with excellent high-temperature mechanical properties (Ref 15). Therefore, the Ti/Al laminate composites have been considered for potential applications in both the aerospace and automobile engines (Ref 16, 17).

Recently, several manufacturing techniques for fabricating Ti/Al laminate composites have been developed, such as roll bonding (Ref 18), vapor deposition (Ref 19) and diffusion bonding (Ref 20). These methods presented disadvantages although proven feasible. During roll bonding process, both the isothermal rolling and the strict control of the process parameters are required, which are both complex and expensive (Ref 21). Additionally, delamination is the most significant serious problem. Therefore, annealing processes are required to be conducted in the next step (Ref 22, 23). The technique of vapor deposition requires sophisticated manufacturing equipment, and large-scale components are significantly slow in preparation (Ref 24). The diffusion bonding will form low-sized voids at the region adjacent to the interface or within the intermetallic layers due to contraction of the metal during interdiffusion, leading to the mechanical properties degradation (Ref 25). The manufacturing technology of the laminate composites proposed in most studies is hot pressing (Ref 16, 26-29). This technology is significantly simple and of low cost. Simultaneously, the components manufactured by this method have both stable and excellent mechanical properties (Ref 15).

As the above-mentioned points described, researchers have devoted attention mainly to the preparation, microstructural characterization and basic mechanical properties of the Ti/Al laminate composites (Ref 6, 7, 30, 31), whereas the Ti/Al laminate composites formability has been studied significantly less. When new parts are prepared by a single operation or several progressive operations, it is very necessary to obtain the attainable forming limit of these materials (Ref 32, 33). Therefore, in this work, the formability of Ti/Al laminate composites was studied, respectively, by uniaxial tension

Liang Qin, College of Material Science and Technology, Nanjing University of Aeronautics and Astronautics, Nanjing 210016, China; and School of Metallurgy and Materials Engineering, Jiangsu University of Science and Technology, Zhangjiagang 215600, China; **Shengqiang Cui**, **Qian Wu**, and **Minyu Fan**, College of Material Science and Technology, Nanjing University of Aeronautics and Astronautics, Nanjing 210016, China; **Zonghui Yang**, Jiangsu Key Laboratory of Advanced Structural Materials and Application Technology, Nanjing 211100, China; and **Jie Tao**, College of Material Science and Technology, Nanjing University of Aeronautics and Astronautics, Nanjing 210016, China; and Jiangsu Key Laboratory of Advanced Structural Materials and Application Technology, Nanjing 211100, China. Contact e-mail: taojie@nuaa.edu.cn.

testing, limit drawing ratio (LDR) and forming limit curve (FLC) experiments.

2. Experimental Procedure

2.1 Preparation and Microstructure Characterization

The dimensions of the cold-worked TA1 titanium and 1060 aluminum foils were of $220 \times 220 \times 0.1$ mm in size (presented in Table 1). The foils were prepared in a vacuum with a controlled temperature, pressure and hot-press duration. Prior to hot pressing, any residual oxides and contaminations on the surface of these Ti and Al foils were removed by the foil submersion in two baths of 60 g/L HF and 150 g/L NaOH solution, respectively. The foils were consequently flushed in both water and ethanol successively. Following a rapid drying, the pretreated foils were stacked into laminates in an alternating sequence of Ti/Al/Ti, with a number of 11 stacks. The typical experimental procedure for the reactive foil bondings in vacuum is schematically presented in Fig. 1. At first, a pressure of 1 MPa was imposed for good contact of each layer inside the vacuum furnace. Following, the temperature was increased to 500 °C in 3 h, whereas the soaking time was 1 h in order for a uniform heating of foils to be ensured. Consequently, the temperature was increased to 550 °C in 0.5 h and retained for 3 h for diffusion bonding of each layer, whereas the pressure was increased to 3 MPa. Finally, the foils were cooled down inside the furnace with the pressure being retained at 1 MPa.

The samples were cut from these Ti/Al laminate composites and mechanically polished down with the 1000 grit abrasive papers and chromium sesquioxide sequentially. The morphology and element distribution of the bonding interface were characterized by a TM 3000 scanning electron microscope with an energy-dispersive spectroscopy (EDS). The phase constituent was observed by the x-ray diffractometry (XRD) which was conducted of a Cu K_{α} radiation source at 40 kV/40 mA.

2.2 Tension Testing

The sub-sized standard tensile specimens were incised from the Ti/Al laminate composites by the wire-electrode cutting, according to the E8 ASTM Standard. The specimen dimension is presented in Fig. 2. The TA1 and 1060Al tensile specimens were also cut according to the same standard. Prior to testing, the samples arc transition was polished smoothly in order to avoid the premature fractures caused by stress concentration. Three tensile tests were completed under various strain rates of 10^{-2} , 10^{-3} and 10^{-4} s^{-1} and measured by a 3542-050M-050-LT extensometer. The experiments of TA1 and 1060Al for comparison were executed under the strain rate of 10^{-3} s^{-1} . The reported data for all the tension tests were the average values of all six tested specimens.

2.3 Limiting Drawing Ratio (LDR)

The LDR tooling geometry schematic is presented in Fig. 3. The deep drawing experiments were performed on the Ti/Al laminate composites, the TA1 and 1060 with the thickness of 1 mm, respectively. During trial testing, the die was statically retained, whereas both the punch and the blank holder were controlled by the hydraulic press. The lubricant, petrolatum, was uniformly smeared on both sides of the specimens prior to experimentation. The blank holder force was a critical experiment parameter and appropriate for the sheet flow, without the sliding permission past the binder and the wrinkling around the punch. In the current tests, the maximum blank holding pressure was 100 kgf/cm². The velocity of the punch was 10 mm/min. The first sample for LDR experimentation had a diameter of 70 mm. The experiment was continued by the gradual diameter increments of 5 mm. The LDR value was defined as the ratio of the diameter which is the largest blank to be successfully formed to the punch diameter. Also, all the reported LDR values were the averaged values of all three tested specimens. Following the deep drawing experiments, the thickness of the final deep drawing cups at various positions was measured by a micrometer [Mitutoyo 0-20 mm (0.001)] and all values were the averaged values of all three tested specimens.

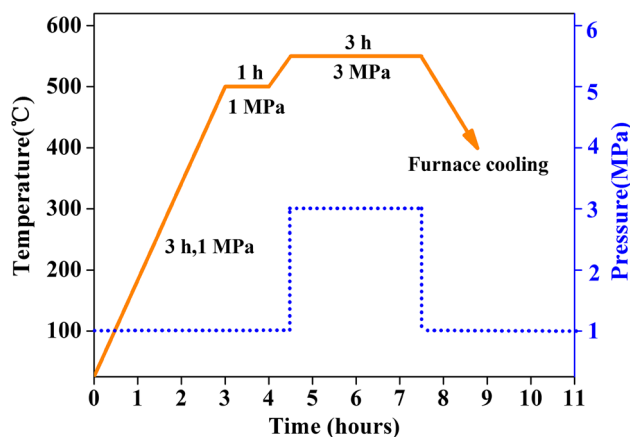


Fig. 1 Experimental procedure for the Ti/Al laminate composites

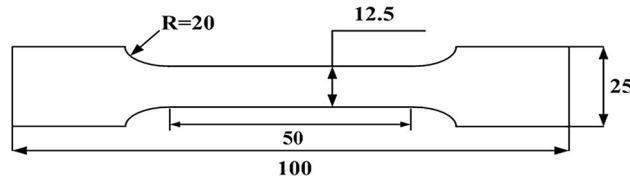


Fig. 2 Dimension of tension specimen

Table 1 Chemical composition and mechanical properties of cold-worked foil materials

Materials	Chemical composition %	Mechanical properties
Titanium TA1	Ti: 99.5, Fe: 0.15, Si: 0.1, O: 0.15 C: 0.05, N: 0.03, H: 0.015	Ultimate: 343 MPa Yield: 275 MPa
Aluminum 1060	Al: 99.16, Fe: 0.35, Si: 0.25, Cu: 0.05 Zn: 0.05, V: 0.05, Mg: 0.03, Mn: 0.03, Ti: 0.03	Ultimate: 100 MPa Yield: 90 MPa

2.4 Forming Limit Curve (FLC)

The FLC experiments were performed for 1060Al and TA1 for comparison. Prior to the FLC experimentation, dot grids were printed on the surface of all 1060, TA1 and Ti/Al laminate composites. The diameters of the printed dot grids were 1 mm, and the in-between gaps of the printed dot grids were 2 mm. The lengths of the specimens were constant 180 mm, whereas the widths varied from 30 to 150 mm. The specimens were deformed into hemispherical domes until fracture. Following fracture, the square comprising a printed four adjacent dots center was transferred into a rhombus. Both the major and minor strains were estimated by the length and width measurement of the rhombus adjacent to the fracture region through an optical strain measurement system. The measurement was conducted from various angles. The forming limit curves were generated by the measured major and minor strains.

3. Results and Discussion

3.1 Microstructure Characterization and Phase Identification

The typical optical cross-section observation of the Ti/Al laminate composites is presented in Fig. 4(a). The interfaces between the combined Ti and Al foils are fairly straight, and low-sized voids are not apparent. Additionally, an approximately 1.5- μm -wide diffusion layer was observed by EDS analysis (presented in Fig. 4b), demonstrating an interdiffusion occurrence between the Ti and Al layers. Figure 5 shows the

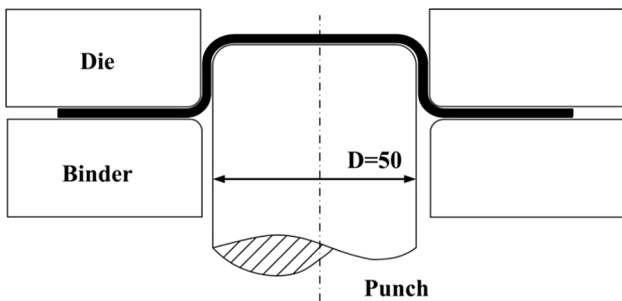


Fig. 3 Tool geometries used in LDR test

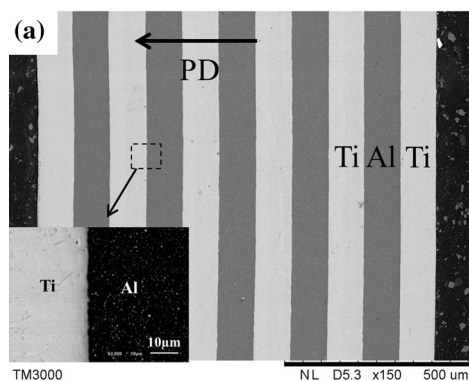


Fig. 4 (a) BSE image of cross section of laminates hot pressed at 550 °C for 3 h; (b) distribution of element at Ti/Al interface

XRD patterns of the cross section of Ti/Al laminated composite. It is noted that the characteristic diffraction peaks of titanium and aluminum are very apparent. However, the peaks of Al_3Ti and other intermetallic compounds do not appear. Therefore, it can be proved that no intermetallic compounds formed on the cross section of existing samples. According to the classic nucleation theory, the formation of a new phase is

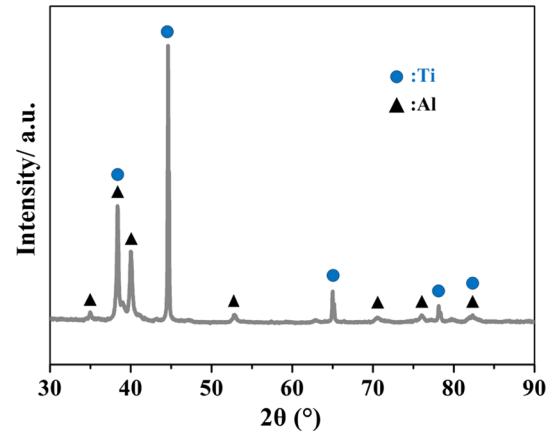


Fig. 5 XRD pattern of the cross section of Ti/Al laminate composite

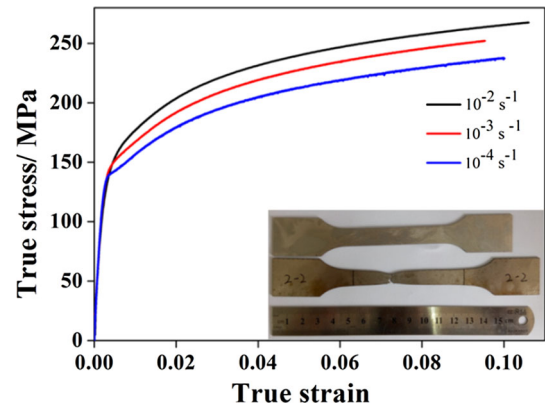
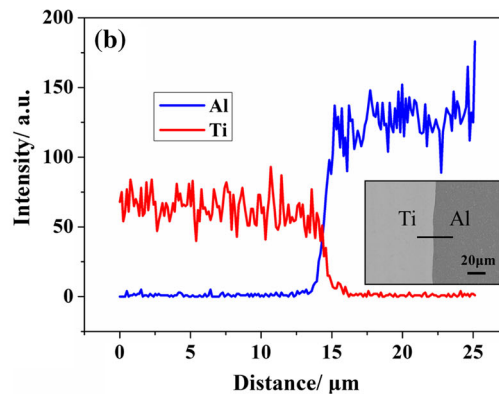


Fig. 6 True stress-strain curves of the Ti/Al laminate composites at several strain rates



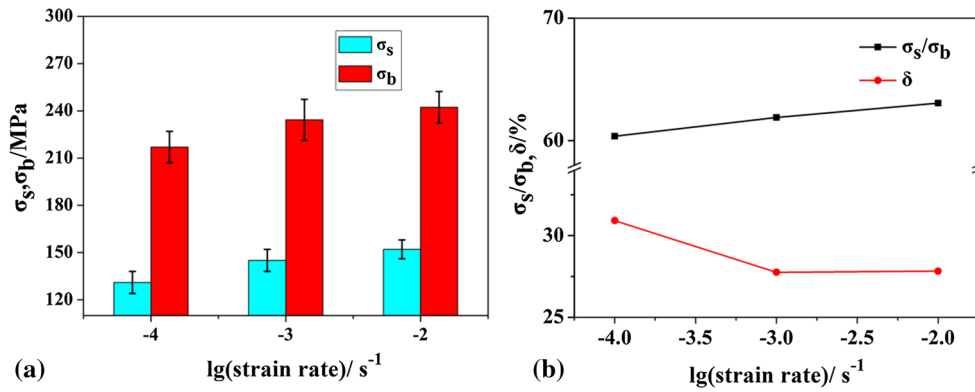


Fig. 7 Tensile properties of the Ti/Al laminate composites under different strain rates

Table 2 The tension results of three materials

Hot pressing	Yield strength, MPa	Tensile strength, MPa	Yield-tensile strength ratio, %	Uniform elongation, %
Ti	355.39	438.93	80.97	12.48
Ti/Al	144.15	234.49	61.47	27.75
Al	18.31	66.60	27.49	46.12

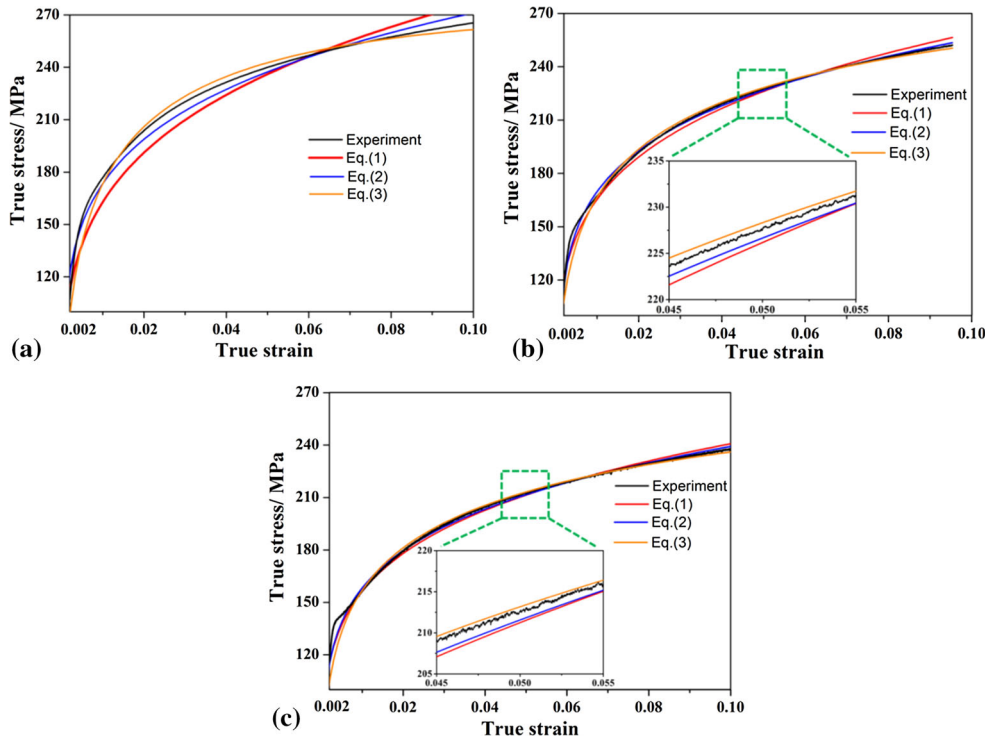


Fig. 8 Fitting curves under different strain rates: (a) $\dot{\epsilon} = 10^{-2} \text{ s}^{-1}$; (b) $\dot{\epsilon} = 10^{-3} \text{ s}^{-1}$; (c) $\dot{\epsilon} = 10^{-4} \text{ s}^{-1}$

determined by not only thermodynamics but also kinetics. At low temperatures, the growth kinetics was probably related to the dominance of the grain boundary diffusion, expected to be slow (Ref 28). At a certain point, it was hard for the intermetallic compounds to nucleate and grow as both the Ti and Al atoms could not widely diffuse through the grain boundary in a short period. It should be pointed out that the bonding was nearly uniform for all interfaces because the entire diffusion occurred at steady pressure with no energy fluctuations.

3.2 Effects of Strain Rate on Tensile Performance

In Fig. 6, the true stress-strain curves of the Ti/Al laminate composites for various strain rates are presented. It is demonstrated that firstly the stress rapidly increased, and then, the increasing rate slowed down along with the increment of strain. Consequently, the curves were less steep. During tensile testing, the slip was the predominant mechanism prior to necking and the slip contributed significantly, following yield comparison to the twinning (Ref 34). The dislocation and corresponding

Table 3 The simulation results of three constitutive equations under different strain rates

Equations	Parameters	10^{-2} s^{-1}	10^{-3} s^{-1}	10^{-4} s^{-1}
$\sigma = K\varepsilon^n$	K	421.9488	363.1514	379.9721
	n	0.1893	0.1511	0.1931
	S	10.6309	1.5749	2.2711
	R	0.9903	0.9951	0.9947
$\sigma = K(\varepsilon_0 + \varepsilon)^n$	K	373.2166	342.361	352.5369
	ε_0	-0.0051	-0.0049	-0.0048
	n	0.1429	0.1264	0.1618
	S	0.2575	0.3916	0.6989
	R	0.9995	0.9988	0.9984
$\sigma = K\varepsilon^{n_1+n_2 \ln \varepsilon}$	K	316.9213	322.6374	304.3435
	n_1	0.0275	0.064	0.07125
	n_2	-0.0218	-0.0175	-0.0162
	S	0.0238	0.043	0.0689
	R	0.9999	0.9999	0.9998

S standard residual dispersion R multiple correlation coefficient

interactions in commercially pure α -Ti phases under tension were elucidated by Kachera et al. (Ref 35) with in situ TEM on the deformations. Therefore, it can be deduced that the stress increased rapidly at the beginning of deformation when slipping was avoided. As the strain increased further, the slipping was gradually overcome, and consequently, the stress increasing rate slowed down. Furthermore, it can be observed in Fig. 6 that the flow stress increases along with the strain rate increment. Simultaneously, as the strain rate increases, the duration of the plastic deformation lessens as a result of the plastic deformation inadequacy. Therefore, the elastic deformation constituted a prominent key factor during total deformation. The yield strength value (approximately 240 MPa) was slightly lower than the yield strength value of pure titanium [approximately 300 MPa in (Ref 32)] at room temperature, due to the lower yield strength value of aluminum, whereas both the titanium and aluminum layers interacted with each other during tensile testing.

Figure 7 shows the tensile properties of the Ti/Al laminate composites under various strain rates (σ_y is the yield strength, σ_b is the tensile strength, and δ is the elongation). Both yield and tensile strengths increase dramatically as the strain rate increases. The increment of the yield-strength ratio and the elongation reduction indicated a plasticity worsening as the strain rate increased. Generally, the utilized metallic elements presented an apparent effect on the strain hardening rate (Ref 36). As the strain rate was extended, the difficulty for dislocation generation deepened and the resistance improved, creating an additional reinforcement on these materials. The aforementioned microphenomenon represented the strength improvement and the plasticity reduction in a macroscopic view. Moreover, all strain rates were in low and middle ranges in the present work. Therefore, the effects of strain rate on the strength and plasticity at room temperature were limited. The results in (Ref 33) displayed that the Ti-6Al-4V alloy presented a high strength (approximately 1100 MPa) at room temperature, whereas the necking was developed quite rapidly when the ultimate tensile strength limit was reached. This behavior was different from the behaviors of pure titanium and even the Ti/Al composites in this research, where the diffuse necking phenomenon occurred prior to fracture. Although the strength

Table 4 The fitted parameters of Eq 3 under different strain rates

$\dot{\varepsilon}$	K	n_1	n_2
10^{-2} s^{-1}	316.9213	0.0275	-0.0218
10^{-3} s^{-1}	322.6374	0.064	-0.0175
10^{-4} s^{-1}	304.3435	0.0712	-0.0162

value was slightly lower in this study, the composites possessed good plastic properties due to coordinated deformation between the titanium and the aluminum layers, during the tensile tests. Furthermore, the tension results of all TA1, 1060Al and Ti/Al laminate composites are listed in Table 2. It can be deduced that during tensile testing, both Ti and Al coordinated the corresponding deformations to each other. Therefore, the yield-tensile strength ratio of these composites was slightly lower than the ratio of Ti, whereas the uniform elongation of the composites was quite higher.

In order to investigate the material fluidity during plastic formation further, the true stress-strain curves were matched to the Hollomon equation Eq 1, the Swift equation (Eq 2) and Eq 3 (Ref 37). As presented in Fig. 8, a comparison among all three constitutive equations is revealed, whereas the third equation coincides well with the true strain-stress curves achieved by uniaxial tension testing. In Fig. 8(b) and (c), some inserts are shown for the details of the curves. It is obviously that the yellow line is closest to the black one. This means the fitting results of Eq 3 are closest to the experiment results. In order for the accuracy of these fitting curves to be ensured, a multiple correlation coefficient R was employed by the experimental data and theoretical prediction comparison. Following the data fitting by the Origin software, the results of these three equations are presented in Table 3. The R values of Eq 3 all exceeded 0.99. This confirms that Eq 3 is a suitable model for the deformation behavior description of the Ti/Al laminate composites at room temperature. The fitted parameters of Eq 3 under various strain rates are listed in Table 4.

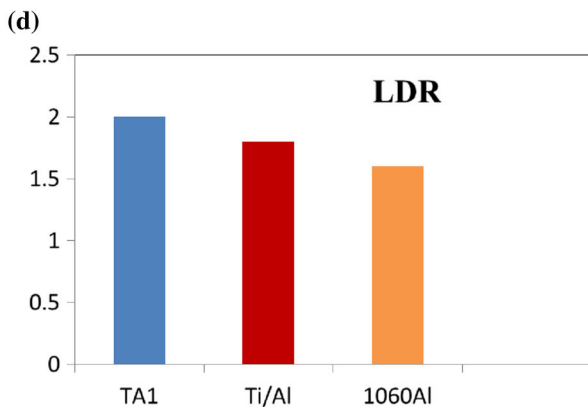
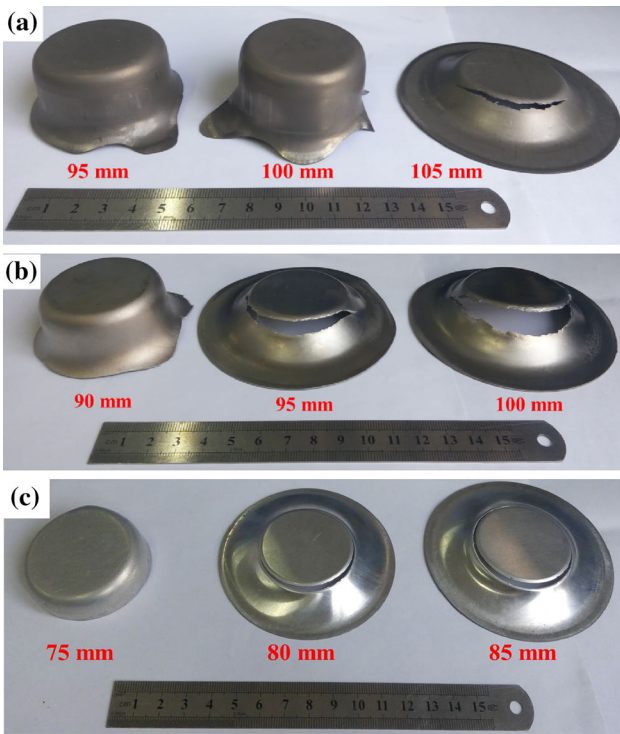


Fig. 9 Deep drawing cups with different sample diameters: (a) TA1 (b) Ti/Al laminate composites (c) 1060Al

$$\sigma = K\varepsilon^n \quad (\text{Eq 1})$$

$$\sigma = K(\varepsilon_0 + \varepsilon)^n \quad (\text{Eq 2})$$

$$\sigma = K\varepsilon^{n_1+n_2 \ln \varepsilon} \quad (\text{Eq 3})$$

where σ and ε are the stress and strain, respectively; K , n , n_1 and n_2 are the constants of the material, measured during the stress-strain curves fitting.

3.3 Forming Performances

The limiting drawing ratio (LDR) is a popular index for the formability of sheet metal description, whereas the higher values of LDR are interpreted as a higher drawing depth and consequently a better formability. The experiment was performed by a sample diameter gradual increase in 5-mm increments, presented in Fig. 9. It can be observed that the best diameters of all TA1, Ti/Al laminate composites and 1060Al samples were 100, 90 and 75 mm, respectively. Subsequently, the LDR values and the thickness strain distribution of Ti/Al were analyzed as presented in Fig. 10. From these deep drawing experiments, it can be observed that the TA1 titanium samples with a maximum diameter of 100 mm could safely be deep drawn into the 50-mm cup. Therefore, calculated according to the equation

$$\text{LDR} = \frac{D_{\max}}{d_p}$$

(D_{\max} is the max diameter value before the fracture appearing at the composite, and the value of d_p is 50 mm), the LDR value of TA1 was 2.0. Similarly, the LDR value of 1060Al was lower than 1.6. Besides, the Ti/Al laminate composites with a maximum diameter of 90 mm were safely deep drawn. Moreover, the corresponding LDR value was 1.8, not being the intermediate LDR value of pure aluminum and titanium. In comparison with the tensile properties during the uniaxial tension test, the formability in the deep drawing was complicated. The forming limit in the deep drawing could not be predicted by the mixture rule, as weighed by volume fractions (Ref 10). It is commonly known that the titanium and aluminum plasticity values differ. Consequently, the coordination

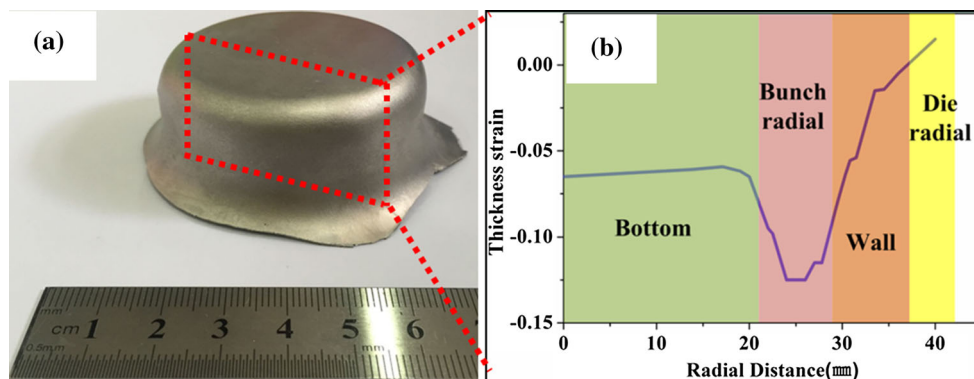


Fig. 10 Drawn cup and distribution of the thickness strain of the Ti/Al laminate composites. (a) drawn cup of the Ti/Al laminate composites; (b) distribution of the thickness strain of the Ti/Al laminate composites

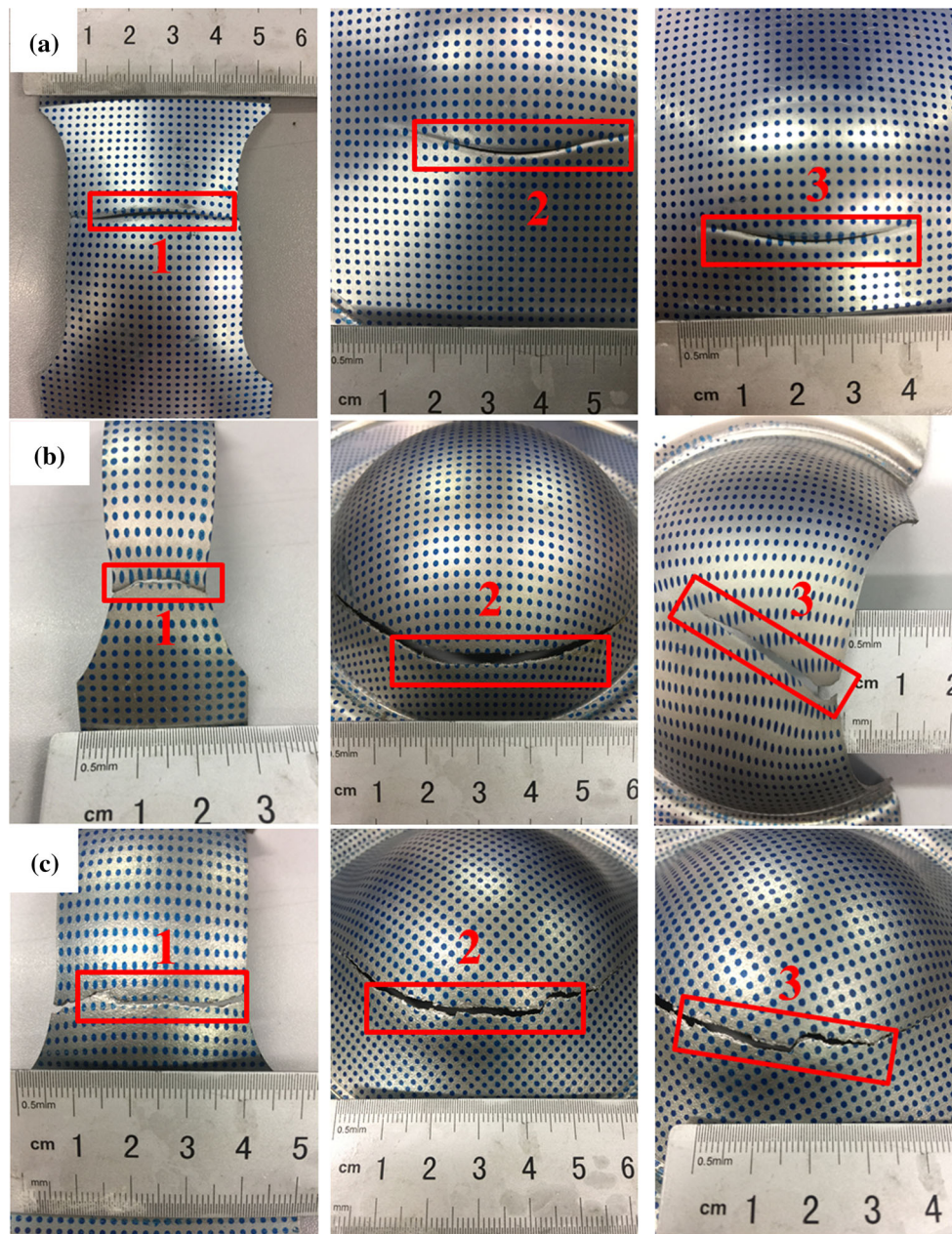


Fig. 11 Forming limit samples after fracture. (a) 1060; (b) TA1; (c) Ti/Al laminate composites

deformation should have been executed between the layers during deep drawing testing. As expected, the LDR value of Ti/Al was in between the LDR values of the TA1 and 1060. Additionally, the fundamental parameters of the Ti/Al laminate composites were the plastic strain ratio (r , $r = \frac{\epsilon_b}{\epsilon_t} = \frac{\epsilon_b}{-(\epsilon_l + \epsilon_b)} = \frac{\ln b / \ln b_0}{-(\ln b / b_0 + \ln l / l_0)} = \frac{\ln b / b_0}{\ln \frac{b_0 l_0}{bl}}$, b_0 is the sample width within the gauge length, b is the sample width within the gauge length after deformation, l_0 is the original gauge length, l is the final gauge length after deformation, ϵ_b is the strain at width direction of the sample, ϵ_t is the strain at thickness direction of the sample, and ϵ_l is the strain at length direction of the sample), the hardening exponent (n , the values of n are obtained by fitting using the Origin software) and the yield-strength ratio (σ_s / σ_b , σ_s is the yield strength, σ_b is the tensile strength), being 1.75, 0.27 and 0.61, respectively, as

obtained from the uniaxial tension tests. These plastic parameters indicated that the deep drawing performance of the Ti/Al laminate composites was really good at room temperature.

One of the most important parameters is the thickness distribution of the final deep drawing cups during the drawing test. High thickness variations resulted in poor quality cups. For this purpose, the drawn cup was sectioned diametrically by a wire cut electric discharge machine. Consequently, the thickness of each layer at various positions from the component centerline was measured by a micrometer. The thickness strain distribution was specified in the radial direction, as presented in Fig. 10(b). The result displayed that the maximum thickness strain of the Ti/Al laminate composites occurred in a radial distance of approximately 25 mm, located almost in the region of the punch profile radius. Badr et al. (Ref 33) discovered that

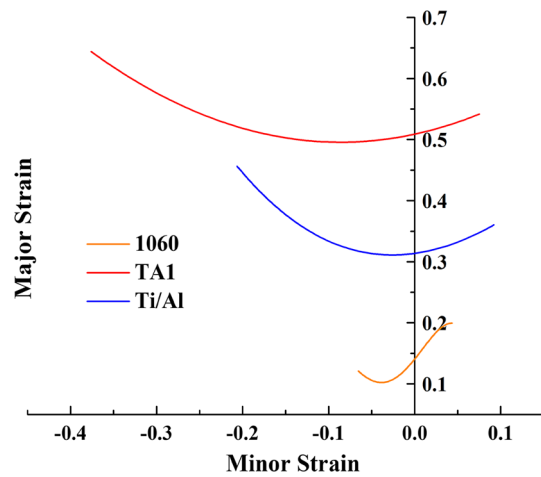


Fig. 12 Experimental forming limit curves at room temperature

the high-strength Ti-6Al-4V alloy presented a limited formability combined with the significantly low material hardening and the high tendency for springback. This suggested that the stamping or deep drawing of the Ti-6Al-4V alloys was not possible at room temperature. Besides, the Ti/Al laminate composites could be deep drawn into complex shape acquisitions at room temperature.

The forming limit constitutes a significant performance index and a process parameter in the sheet metal forming field. The fractures in forming limit samples are presented in Fig. 11, including the details of the fracture shown as Positions 3. It can be observed that the forming height was significantly high and the Ti/Al laminate composites thickness near the crack was apparently thinning, displaying the ductile fracture (Fig. 11c). Additionally, the cracks of the 1060 and TA1 were mostly straight as shown in Fig. 11(a) and (b), respectively. In contrast, the annular cracks of the laminate composites presented a saw-tooth shape, concentrated at the bottom (Fig. 11c). As a rule, the cracks always extend following the maximum principal stress criterion. The samples were in a complex stress state due to the effects of the external load along with the interactions between the layers of the Ti/Al laminate composites during deformation. Therefore during testing, the sample danger zone had almost the same mechanical properties throughout all directions.

The measurement was conducted from various angles at 0°, 45°, 90°, 135°, 180°, 225°, 270°, 315° and 360°. Also, the major and minor strains were experimentally obtained through repeated measurements. The cubic polynomial interpolation was employed for the forming limit curves fitting. The forming limit curves of all TA1, 1060 and Ti/Al laminate composites are presented in Fig. 12. It can be observed that the FLC of the latter laminate composites existed between the FLC values of the 1060 and TA1. Besides, the FLC of the Ti/Al laminate composites intersects with the major strain line approximately at 0.31, similar to the work hardening exponent of this material at room temperature. Moreover, in the biaxial strain region, the FLC slope of the Ti/Al laminate composites was lower. In this region, the major and minor strains were positive numbers; therefore, the surface area of the Ti/Al laminate composites increased. According to the volume constancy principle, the samples were mainly deformed by thinning. Besides, in the uniaxial strain region, the major and minor strains were positive

and negative numbers, respectively. The samples could flow to either side freely, postponing the destabilization caused by thinning.

4. Conclusions

1. The Ti/Al laminate composites with good bonding interfaces between Ti and Al layers were prepared by hot pressing, and no low-sized voids and intermetallic compounds were formed at the interfaces.
2. The strain rate increment had a positive effect on the flow stress of Ti/Al laminate composites. Besides, the elongation slightly reduced as the strain rate increased. The constitutive equation $\sigma = K\epsilon^{n_1+n_2 \ln \epsilon}$ was a suitable model for the deformation behavioral description of the Ti/Al laminate composites.
3. The Ti/Al laminate composites presented a good deep drawing performance and the LDR was 1.8. Distribution of thickness strain in the drawn cup indicated that the most susceptible region to fracture was located at the punch profile radius.
4. The FLC of the Ti/Al laminate composites was located between the FLC values of 1060 and TA1 and intersected the major strain line approximately at 0.31, being similar to the work hardening exponent. The macroscopic cracks of FLC samples presented a saw-toothed crack feature during testing.

Acknowledgments

The authors gratefully acknowledge the financial support of the National Natural Science Foundation of China (No. 51475231), a Project Funded by the Priority Academic Program Development of Jiangsu Higher Education Institutions, the Funding of Jiangsu Innovation Program for Graduate Education (No. KYLX_0263), Foundation of Graduate Innovation Center in NUAA (kfj20150606) and the Fundamental Research Funds for the Central Universities (No. 20150027).

References

1. B. Zhang, Y. Kou, Y.Y. Xia, and X. Zhang, Modulation of Strength and Plasticity of Multiscale Ni/Cu Laminated Composites, *Mater. Sci. Eng. A*, 2015, **636**, p 216–220
2. Y.E. Qi, Y.S. Zhang, and L.T. Hu, High-Temperature Self-lubricated Properties of Al₂O₃/Mo Laminated Composites, *Wear*, 2012, **280**, p 1–4
3. R.O. Ritchie, The Conflicts Between Strength and Toughness, *Nat. Mater.*, 2011, **10**(11), p 817–822
4. K. Zhu, W.B. Yu, Y. Aman, and T. Jing, Synthesis, Microstructure and Mechanical Properties of a Bio-Inspired Ti-Intermetallic Multi-layered/SiC_f-reinforced Ti-Matrix Hybrid Composite, *J. Mater. Sci.*, 2016, **51**(18), p 8747–8760
5. M.Y. Fan, J. Domblesky, K. Jin, L. Qin, S.Q. Cui, X.Z. Guo, N. Kim, and J. Tao, Effect of Original Layer Thicknesses on the Interface Bonding and Mechanical Properties of Ti-Al Laminate Composites, *Mater. Des.*, 2016, **99**, p 535–542
6. M. Ma, P. Huo, W.C. Liu, G.J. Wang, and D.M. Wang, Microstructure and Mechanical Properties of Al/Ti/Al Laminated Composites Prepared by Roll Bonding, *Mater. Sci. Eng. A*, 2015, **636**, p 301–310
7. D.V. Lazurenko, I.A. Bataev, V.I. Mali, A.A. Bataev, I.N. Maliutina, V.S. Lozhkin, M.A. Esikov, and A.M.J. Jorge, Explosively Welded

- Multilayer Ti-Al Composites: Structure and Transformation During Heat Treatment, *Mater. Des.*, 2016, **102**, p 122–130
8. F.T. Kong, Y.Y. Chen, and D.L. Zhang, Interfacial Microstructure and Shear Strength of Ti–6Al–4V/TiAl Laminate Composite Sheet Fabricated by Hot Packed Rolling, *Mater. Des.*, 2011, **32**, p 3167–3172
 9. M. Samavatian, A. Halvaei, A. Amadeh, and S. Zakipour, Microstructure and Mechanical Properties of Al2024/Ti-6Al-4V Transient Liquid Phase Bonded Joint, *J. Mater. Eng. Perform.*, 2015, **24**(6), p 2526–2534
 10. S. Chatterjee, A. Sinha, D. Das, S. Ghosh, and A. Basumallick, Microstructure and Mechanical Properties of Al/Fe-aluminide In situ Composite Prepared by Reactive Stir Casting Route, *Mater. Sci. Eng. A*, 2013, **578**, p 6–13
 11. A. Dziadoń, R. Mola, and L. Błaż, Formation of Layered Mg/eutectic Composite Using Diffusional Processes at the Mg-Al Interface, *Arch. Metal. Mater.*, 2011, **56**(3), p 677–684
 12. P.J. Lee, A.A. Squitieri, D.C. Larbalestier, T. Takeuchi, N. Banno, T. Fukuzaki, and H. Wada, Microchemical and Microstructural Comparison of High Performance Nb₃Al Composites, *IEEE Trans. Appl. Supercond.*, 2003, **13**(2), p 3398–3401
 13. Y. Guo, G. Liu, H. Jin, Z. Shi, and G. Qiao, Intermetallic Phase Formation in Diffusion-Bonded Cu/Al Laminates, *J. Mater. Sci.*, 2011, **46**(8), p 2467–2473
 14. M. Konieczny, Processing and Microstructural Characterisation of Laminated Ti-Intermetallic Composites Synthesised Using Ti and Cu Foils, *Mater. Lett.*, 2008, **62**(17), p 2600–2602
 15. I.A. Bataev, A.A. Bataev, V.I. Mali, and D.V. Pavliukovaa, Structural and Mechanical Properties of Metallic–Intermetallic Laminate Composites Produced by Explosive Welding and Annealing, *Mater. Des.*, 2012, **35**, p 225–234
 16. J.P. Liu, L.S. Luo, Y.Q. Su, Y.J. Xu, X.Z. Li, R.R. Chen, J.J. Guo, and H.Z. Fu, Numerical Simulation of Intermediate Phase Growth in Ti/Al Alternate Foils, *Trans. Nonferr. Met. Soc.*, 2011, **21**(3), p 598–603
 17. X. Wu, Review of Alloy and Process Development of TiAl Alloys, *Intermetallics*, 2006, **14**(10), p 1114–1122
 18. K. Kothari, R. Radhakrishnan, and N.M. Wereley, Advances in Gamma Titanium Aluminides and Their Manufacturing Techniques, *Prog. Aerosp. Sci.*, 2012, **55**, p 1–16
 19. J.P. Liu, Y.Q. Su, L.S. Luo, H. Chen, Y.J. Xu, J.J. Guo, and H.Z. Fu, Fabrication of Wavy γ -TiAl Based Sheet with Foil Metallurgy, *Trans. Nonferr. Met. Soc.*, 2012, **22**(1), p 72–77
 20. L.I. Duarte, F. Viana, A.S. Ramos, M.T. Vieira, C. Leinenbach, U.E. Klotz, and M.F. Vieira, Diffusion Bonding of γ -TiAl Using Modified Ti/Al Nanolayers, *J. Alloy. Compd.*, 2012, **536**, p 424–427
 21. R.K. Gupta, B. Pant, and P.P. Sinha, Theory and Practice of $\gamma + \alpha_2$ Ti Aluminide: A Review, *Trans. Indian Met.*, 2014, **67**(2), p 143–165
 22. A.H. Assari and B. Eghbali, Interfacial Layers Evolution During Annealing in Ti-Al Multi-laminated Composite Processed Using Hot Press and Roll Bonding, *Met. Mater. Int.*, 2016, **22**(5), p 915–923
 23. H.L. Yu, C. Lu, A.K. Tieu, H.J. Li, A. Godbole, and C.L. Kong, Annealing Effect on Microstructure and Mechanical Properties of Al/Ti/Al Laminate Sheets, *Mater. Sci. Eng. A*, 2016, **660**, p 159–204
 24. D.E. Alman, J.A. Hawk, A.V. Petty, Jr., and J.C. Rawers, Processing Intermetallic Composites by Self-propagating, High-Temperature Synthesis, *JOM*, 1994, **46**(3), p 31–35
 25. F. Kong, Y. Chen, and D. Zhang, Interfacial Microstructure and Shear Strength of Ti-6Al-4V/TiAl Laminate Composite Sheet Fabricated by Hot Packed Rolling, *Mater. Des.*, 2011, **32**(6), p 3167–3172
 26. J. Liu, Y. Su, Y. Xu, L. Luo, J. Guo, and H. Fu, First Phase Selection in Solid Ti/Al Diffusion Couple, *Rare Met. Mater. Eng.*, 2011, **40**, p 753–756
 27. Y. Wei, W. Aiping, Z. Guisheng, and R. Jialie, Formation Process of the Bonding Joint in Ti/Al Diffusion Bonding, *Mater. Sci. Eng. A*, 2008, **480**, p 456–463
 28. L. Xu, Y.Y. Cui, Y.L. Hao, and R. Yang, Growth of Intermetallic Layer in Multi-laminated Ti/Al Diffusion Couples, *Mater. Sci. Eng. A*, 2006, **435–436**, p 638–647
 29. Y.B. Sun, Y.Q. Zhao, D. Zhang, C.Y. Liu, H.Y. Diao, and C.L. Ma, Multilayered Ti-Al Intermetallic Sheets Fabricated by Cold Rolling and Annealing of Titanium and Aluminum Foils, *Trans. Nonferr. Met. Soc.*, 2011, **21**, p 1722–1727
 30. Y.B. Sun, M.W. Liu, S.J. Ge, F.M. Ma, and C.L. Ma, Preparation of Multilayered Ti-Al Intermetallic Sheets Fabricated by Solid Reaction, *Mater. Sci. Forum*, 2013, **747–748**, p 1–8
 31. Y. Du, G.H. Fan, T.B. Yu, N. Hansen, L. Geng, and X.X. Huang, Laminated Ti-Al Composites: Processing, Structure and Strength, *Mater. Sci. Eng. A*, 2016, **673**, p 572–580
 32. F.K. Chen and K.H. Chiu, Stamping Formability of Pure Titanium Sheets, *Mater. Process. Technol.*, 2005, **170**, p 181–186
 33. O.M. Badr, B. Rolfe, P. Hodgson, and M. Weiss, Forming of High Strength Titanium Sheet at Room Temperature, *Mater. Des.*, 2015, **66**, p 618–626
 34. L.F. Li, Z. Zhang, and G.T. Shen, Effect of Grain Size on the Tensile Deformation Mechanisms of Commercial Pure Titanium as Revealed by Acoustic Emission, *JMEP*, 2015, **24**, p 1975–1986
 35. J. Kachera and I.M. Robertson, In situ TEM Characterisation of Dislocation Interactions in α -titanium, *Philos. Mag.*, 2016, **96**(14), p 1437–1447
 36. A.S. Khan and H. Liu, Strain Rate and Temperature Dependent Fracture Criteria for Isotropic and Anisotropic Metals, *Int. J. Plast.*, 2012, **37**, p 1–15
 37. X. Tian and Y. Zhang, Mathematical Description for Flow Curves of Some Stable Austenitic Steels, *Mater. Sci. Eng. A*, 1994, **174**(1), p 1–3